Heriot-Watt University
Research Gateway

Analysis and Design of Dual-Band Folded-Shorted Patch Antennas for Robust Wearable Applications

Citation for published version:
Joshi, R, Podilchak, SK, Anagnostou, DE, Constantinides, C, Ramli, MN, Lago, H & Soh, PJ 2020, 'Analysis and Design of Dual-Band Folded-Shorted Patch Antennas for Robust Wearable Applications', *IEEE Open Journal of Antennas and Propagation*, vol. 1, pp. 239-252. https://doi.org/10.1109/OJAP.2020.2991343

Digital Object Identifier (DOI):
10.1109/OJAP.2020.2991343

Link:
Link to publication record in Heriot-Watt Research Portal

Document Version:
Publisher's PDF, also known as Version of record

Published In:
IEEE Open Journal of Antennas and Propagation

General rights
Copyright for the publications made accessible via Heriot-Watt Research Portal is retained by the author(s) and / or other copyright owners and it is a condition of accessing these publications that users recognise and abide by the legal requirements associated with these rights.

Take down policy
Heriot-Watt University has made every reasonable effort to ensure that the content in Heriot-Watt Research Portal complies with UK legislation. If you believe that the public display of this file breaches copyright please contact open.access@hw.ac.uk providing details, and we will remove access to the work immediately and investigate your claim.

Download date: 14. Jul. 2025

Received 27 February 2020; revised 30 March 2020; accepted 17 April 2020. Date of publication 29 April 2020; date of current version 15 June 2020.

Digital Object Identifier 10.1109/OJAP.2020.2991343

Analysis and Design of Dual-Band Folded-Shorted Patch Antennas for Robust Wearable Applications

RAHIL JOSHI[1,2], SYMON K. PODILCHAK[2] (Member, IEEE), DIMITRIS E. ANAGNOSTOU[1] (Senior Member, IEEE), CONSTANTIN CONSTANTINIDES[1], MUHAMMAD NAZRIN RAMLI[3], HERWANSYAH LAGO[3], AND PING JACK SOH[3] (Senior Member, IEEE)

[1]Insititute of Sensors, Signals and Systems, Heriot-Watt University, Edinburgh EH14 4AS, U.K.

[2]Institute for Digital Communications, School of Engineering, University of Edinburgh, Edinburgh EH8 9YL, U.K.

[3]Advanced Communication Engineering Centre, School of Computer and Communication Engineering, Universiti Malaysia Perlis, Arau 02600, Malaysia

CORRESPONDING AUTHOR: S. K. PODILCHAK (e-mail: s.podilchak@ed.ac.uk).

This work was supported in part by the European Union's Horizon 2020 Research and Innovation Program through Marie Sklodowska-Curie under Grant #709372, the EU H2020 ITN REVOLVE Project under Grant #722840, and in part by the EU H2020 Individual Fellowship #840854 ViSionRF.

ABSTRACT A flexible folded-shorted patch (FSP) antenna with dual-band functionality for wearable applications is presented. The proposed antenna is operational at 400 MHz and 2.4 GHz and can be considered compact for the lower operational frequency band ($0.13\lambda_o \times 0.13\lambda_o \times 0.02\lambda_o$). Flexible polydimethylsiloxane (PDMS) is used as the substrate due to its relatively low-cost as well as its robustness for wearable applications. A comparison of the fields radiated by the FSP, in terms of the TM_{010} and TM_{001} modes are also presented considering the cavity model which is actually related to the two noted operating bands. Equations needed to calculate the beam pattern and directivity for these modes are also derived and their results are compared to commercial full-wave simulations and measurements of a wearable PDMS prototype. An analysis was also performed to characterize the relevant dimensions that are important for independently controlling or tuning the resonant frequencies for these two radiating modes. The proposed antenna can be suitable for robust wearable applications such as military search and rescue operations, emergency response team units, and medical services.

INDEX TERMS Folded-shorted patch (FSP) antenna, wearable antennas, TM modes.

I. INTRODUCTION

WEARABLE antennas in recent years have advanced significantly and been researched for various applications. Healthcare, defence, retail and transportation are several possible sectors where these antennas can be beneficial. Furthermore, these antennas will play a vital role in ongoing and future wearable communication systems. Some of the textile-based devices which are available commercially include wearable sensor jackets and sensor badges [1], sensor T-shirts [2] and Smart Vests [3]. Other wearable products that are used by consumers in day to day life are smart glasses, health and tracking wristbands and smart watches.

The proposed wearable antenna in this paper is designed and fabricated for military search and rescue operations and emergency services and provides dual-band functionality, but is also suitable for other applications which require wearable transceivers. Figure 1 provides an illustration of such a wearable antenna system positioned in a ballistics jacket which can enable UHF satellite beacon signal links for geolocation as well as Bluetooth and Wi-Fi communications. Previous and more commercially available beacon signal UHF devices were hand held and bulky with classic monopole antennas of length $\lambda/4$. At the UHF band the proposed antenna of this work is $0.13\lambda_o$ by $0.05\lambda_o$ by $0.02\lambda_o$ making it electrically compact, while at the second 2.45 GHz band, the antenna has the largest impedance fractional bandwidth (FBW) and smallest form factor when compared to similar dual-band antennas (see Table 1). Other applications include integration within the clothing of emergency fire and medical teams and medical service workers.

To the authors' best knowledge, no similar antenna structure has been reported with a dedicated design methodology

This work is licensed under a Creative Commons Attribution 4.0 License. For more information, see https://creativecommons.org/licenses/by/4.0/

TABLE 1. Comparison of other FSP structures found in the literature.

Parameter	[21]	[22]	[24]	[27]	This Work
	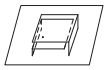	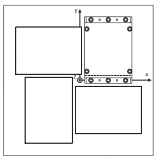	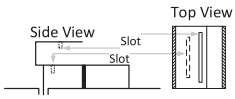	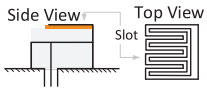	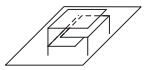
Number of Layers	2 Layers	4 Layers with 4 elements	2 Layers	2 Layers	3 Layers
Frequency	2.4 GHz	400 MHz	823 MHz / 2.194 GHz	2.4 GHz / 5 GHz	400 MHz / 2.4 GHz
Single-element Size	$0.15\lambda_o \times 0.08\lambda_o \times 0.02\lambda_o$	$0.05\lambda_o \times 0.04\lambda_o \times 0.05\lambda_o$	$0.45\lambda_o \times 0.34\lambda_o \times 0.06\lambda_o$ / $1.185\lambda_o \times 0.926\lambda_o \times 0.176\lambda_o$	$0.1\lambda_o \times 0.01\lambda_o \times 0.05\lambda_o$ / $0.316\lambda_o \times 0.208\lambda_o \times 0.079\lambda_o$	$0.13\lambda_o \times 0.05\lambda_o \times 0.02\lambda_0$ / $0.816\lambda_o \times 0.32\lambda_o \times 0.16\lambda_o$
Single-element Volume	$0.00024\lambda_o^3$	$0.0001\lambda_o^3$	$0.0091\lambda_o^3$ / $0.193\lambda_o^3$	$0.00005\lambda_o^3$ / $0.0051\lambda_o^3$	$0.00013\lambda_o^3$ / $0.0417\lambda_o^3$
Ground-plane Dimensions	$0.12\lambda_o \times 0.12\lambda_o$	$0.2\lambda_o \times 0.2\lambda_o$	$0.25\lambda_o \times 0.36\lambda_o$ / $2.06\lambda_o \times 2.338\lambda_o$	$0.3\lambda_o \times 0.3\lambda_o$ / $0.62\lambda_o \times 0.62\lambda_o$	$0.27\lambda_o \times 0.27\lambda_o$ / $1.6\lambda_o \times 1.6\lambda_o$
Polarization	Linear	Circular	Linear	Linear	Linear
Modes	TM_{010}	TM_{010}	TM_{010} / TM_{030}	TM_{010} / TM_{030}	TM_{010} / TM_{001}
Maximum Realized Gain	3.0 (dBi)	2.5 (dBic)	5.0 / 6.0 (dBi)	2.1 / 5.3 (dBi)	1.4 / 3.1 (dBi)
Impedance FBW[1]	3.6%	4.0%	21.0% / 32.2%	0.8% / 3.4%	3.5% / 7.3%

[1]The impedance fractional bandwidth (FBW), where $|S_{11}| \leq$ -10 dB, was computed using the equation identified in ([28], Ch 11, eq 11.36) where $FBW = (F_H - F_L)/F_c \times 100$, F_H is the highest frequency, F_L is the lowest frequency and F_c is the centre frequency.

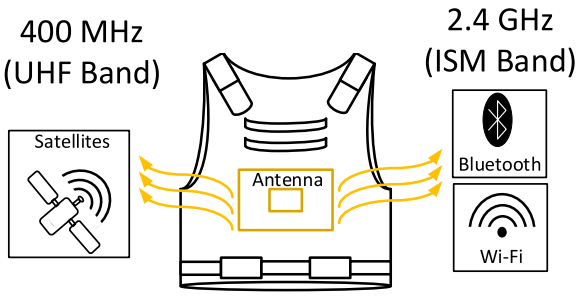

FIGURE 1. Illustration of a wearable antenna and integration into clothing; i.e., a ballistics jacket for military search and rescue activities to enable simple satellite communications, where the operator can be found using a beacon, and other wireless applications such as Bluetooth and Wi-Fi at 2.4 GHz for connectivity to local area networks.

and a supporting analysis describing antenna operation. Also keeping in mind that military and emergency services personnel wear heavy equipment, the antenna design approach developed in this work is slightly different from more conventional wearable antennas. To be specific, the antenna needs to be comfortable for the user to wear, hence it needs to be relatively compact and low-profile. Flexibility and robustness are also some of the essential characteristics. To provide flexibility to the antenna a textile or polymer-based material is a good candidate and is chosen as the antenna substrate in this work. Since the size of the antenna should be compact with respect to the wavelength, a miniaturized structure is preferred. Also, the designed antenna should offer efficient radiation in any environment and be robust.

It should also be mentioned that several wearable antennas of different shapes and sizes were developed over the past few years offering both single-frequency and multi-band operation. These include a dual-band button shaped antenna [4], watch strap antennas [5] and logo shaped wearable antennas [6]. In [7], different types of antennas along with various substrate materials were also reviewed. For search and rescue operations antennas such as the bowtie and spiral [8], the shorted patch [9], and a circular ring-like patch with truncated corners [10] have been previously developed and reported. In addition, wearable antennas have also developed by employing electromagnetic bandgap (EBG) [11] and artificial magnetic conductor (AMC) [12] planes to improve antenna radiation away from the body.

When considering wearable antennas operating at the UHF and the ISM band, patch-like antennas are generally preferred due to their low profile, possible miniaturization approaches, and relatively low cost implementations. There are several size reduction techniques for the conventional patch antenna which have been developed and implemented. Some of these techniques use high dielectric materials [13]–[15], introducing slots in the design [16]–[18], bending and folding of the planar elements [19], and lumped element loading.

The bending and folding technique or the addition of a metallic shorting wall is one effective method. As is well known, folded antennas such as the inverted-F antenna (IFA) and the planar inverted-F antenna (PIFA) are used widely for many applications and are typically a quarter wavelength in the size when only considering the antenna itself [19], [20].

However, the size of the PIFA can be further reduced to less than $\lambda/4$ by folding the patch element further into multiple layers and forming a multilayer structure. This structure is generally two or more layers defining a folded-shorted patch (FSP) antenna.

The concept of the FSP antenna was originally introduced in [21] and developed further in [22] and [23]. Following these earlier developments a dual-band FSP was proposed for operation at about 800 MHz and 2.2 GHz [24]. Preliminary results were reported by the authors in [25] for a simple and single-layer circularly polarized (CP) patch antenna where durability and resiliency studies were completed for the adopted polydimethylsiloxane (PDMS) substrate in terms of bending, wet and temperature testing. Results suggest that such an antenna can withstand these operational conditions and without significant performance degradations in terms of variations in impedance matching and antenna gain. Following these developments some preliminary results for a three-layer FSP using PDMS were reported in [26] considering its potential for dual-band functionality. Concepts and antenna analysis is further explained in this paper for a new and optimized, dual-band antenna unit which can operate at about 400 MHz and 2.4 GHz, and where the relevant radiating modes are fully explained and the benefits of these patch modes (see Fig. 2) are discussed when compared to previously reported antenna structures.

The proposed FSP design in this paper is simple, achieving broadside radiation, requires no slots, is flexible for wearable applications, and newly exploits the TM_{001} mode for the FSP. The paper is organized as follows. In Section II, the design motivation of the proposed FSP antenna is described while also providing a literature review on previous reported FSP antennas. In Sections III and IV, the material selection process, antenna miniaturization, and assembly are discussed. The modes of the proposed FSP are also analyzed and comparisons are made to a single-layer patch. Measurements of the antenna reflection coefficient and radiation pattern are discussed in Section V while some conclusions are made in Section VI.

II. ANTENNA DESIGN OVERVIEW AND MOTIVATION

The proposed PDMS antenna in this paper exploits the TM_{010} and the TM_{001} modes of the FSP and these modes are achieved without the introduction of slots, as in [24] and [27], where the FSP antennas operated by the TM_{010} and TM_{030} modes. This can make the antenna design simpler and easier to fabricate when considering the TM_{010} and the TM_{001} modes as in this work. More importantly, the TM_{030} mode and other higher order modes can exhibit unwanted nulls in the beam pattern [28] (see pattern simulations in Fig. 2 where a comparison of these modes is provided) which might not be appropriate for the intended wearable application.

It should also be mentioned that for the higher order TM_{001} mode, the fields radiate from the opposite edges of the antenna when compared to the TM_{010} mode by the cavity model for the single-layer patch [28]. As a consequence,

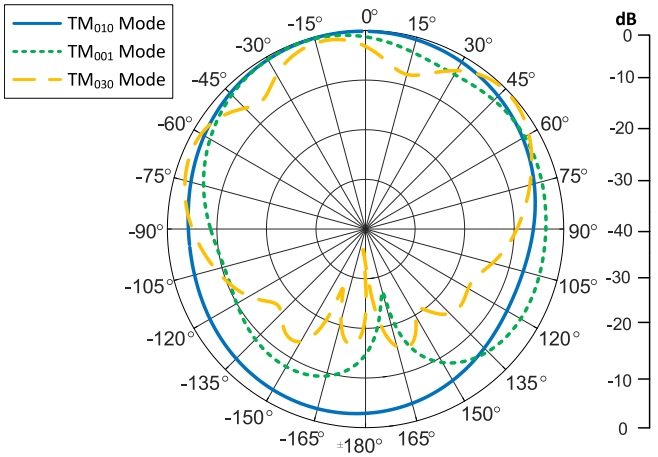

FIGURE 2. Beam pattern at the TM_{010}, TM_{001} and TM_{030} modes for a three-layer FSP antenna. The TM_{030} modes has multiple side lobes whereas other two modes have a more omnidirectional-like pattern with broadside radiation.

the polarization of the FSP changes but it still maintains broadside radiation and with reduced side lobe levels. Also, the FSP structure proposed in this paper is without slots, which can lead to unperturbed current paths [29] for both the TM_{010} and the TM_{001} modes. This supports sustained broadside radiation. Due to these important design considerations, the proposed FSP structure has two operational frequencies with orthogonal polarization. This is achieved using a single feed point as described previously in [29] for a more conventional patch.

These modes are further examined in this paper when compared to other similar works [24] and [27], mainly, the proposed antenna is analyzed and designed by employing the cavity model for the conventional patch [28], [30] and applying it to a multi-layer FSP. In the forthcoming sections closed-form equations are newly derived to calculate the beam pattern and the directivity. Results are validated by comparisons between theory, full-wave simulations, and measurements. The developed analysis approach, specifically for FSPs, easily allows the antenna engineer to estimate the operational frequency, pattern shape, polarization, and directivity prior to any simulation and fabrication activity. This can help to reduce design and optimization time.

The proposed FSP antenna is also relatively smaller in size compared to the designs reported in [21], [22], [24] and [27] when considering the first operating mode. In this work, dual frequency operation is achieved by tuning the size of the layers of the FSP antenna. Also, the top layer of the proposed FSP antenna is proportional to the TM_{010} mode and by varying the size of the top layer (layer 3, see Fig. 3) one can tune the frequency of the dominant (TM_{010}) mode. Also, it was found out that the other two layers (layer 1 and layer 2, see Fig. 3) are proportional to the higher order TM_{001} mode. As further described in this paper, the TM_{001} mode can be tuned to a particular frequency while the TM_{010} mode is maintained.

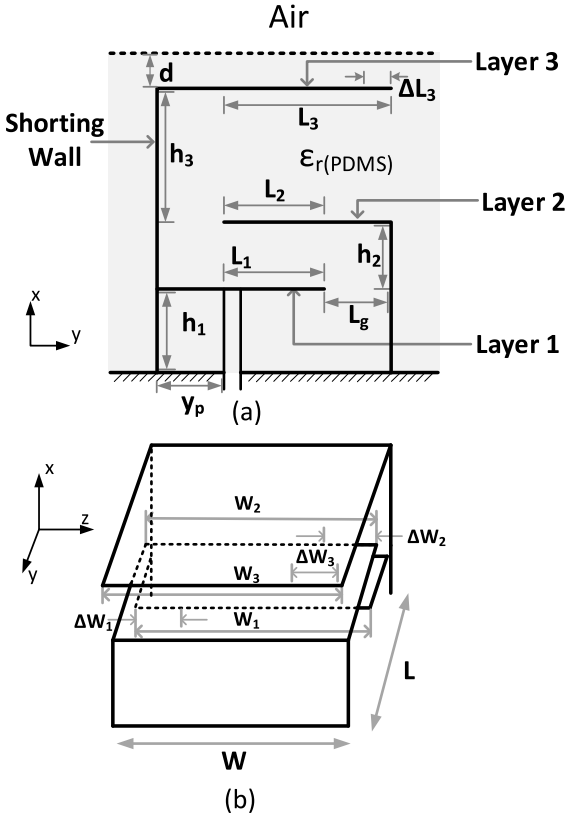

FIGURE 3. (a) A cross-sectional view of a three-layer FSP considering a PDMS substrate. y_p denotes the distance of the probe from the shorting wall in the y-direction. (b) W_1, W_2, and W_3 are the width of the three layers for the FSP. ΔW_1, ΔW_2, ΔW_3 and ΔL_3 are the parameters altered in the tuning analysis (see Section IV).

Table 1 summaries the advantages of the proposed FSP antenna as compared to other designs reported in the literature. For example, the impedance fractional bandwidth (FBW) of the proposed antenna both at the dominant (400 MHz) mode (UHF band frequency range) and at the higher order (2.4 GHz) mode (ISM band frequency range) is larger than in [27]. It should also be mentioned that in [24] slots were used to enhance the bandwidth (BW) of the FSP antenna and making it a multiband antenna. This approach with slot inclusions can possibly increase the design complexity. The proposed FSP antenna in this work has a simple geometry without any slots and yet is still able to offer a FBW of more than 7% at the higher order mode. At 400 MHz, the FBW is 3.5% (and is still larger than [27] for the fundamental mode). It is also worth mentioning here that for this TM_{010} mode the proposed FSP is compact ($0.13\ \lambda_o \times 0.13\lambda_o \times 0.02\lambda_o$) and when considering the ground plane size when compared to [24] and [27]. The relatively narrow impedance FBW of 3.5% at 400 MHz, means that the wearable antenna can work as a beacon antenna for telemetry applications since low data rates are required. Also, the proposed FSP antenna has a relatively smaller single element footprint and volume as compared to the designs reported in [21], [24], [27] for the TM_{010} mode (see Table 1).

III. WEARABLE ANTENNA SUBSTRATE CONSIDERATIONS

It is known that several properties can influence antenna behaviour. For instance, the BW and the efficiency of a microstrip antenna are mainly determined by the permittivity and the thickness of the substrate. Wearable antennas should be durable and resilient to such a harsh environment and especially when considering the applications of military and search and rescue operations. One potential material that could meet the specification of a wearable antenna is polydimethylsiloxane (PDMS). The low loss (tan $\delta = 0.03$ from 0.2 GHz to 5 GHz) [31], low dielectric constant ($\epsilon_r = 2.76$ from 0.2 GHz to 5 GHz) [31], flame resistant and hydrophobic properties [32] also makes PDMS appealing for wearable applications. More importantly, the hydrophobic characteristic of PDMS makes it stable across a wide range of environments by preventing changes in the relative dielectric constant and loss tangent.

PDMS is also preferable when compared to conventional textile materials because it is waterproof, weatherproof, low cost, easy to fabricate, has a low permittivity, and is flexible. The practical adhesion between metal and such a polymer; i.e., PDMS can be challenging but can be improved by using methods such as using copper meshes or perforated metal plates as a conductive part of the antenna [31], embedding high density carbon nanotubes within the polymer to achieve carbon nanotube sheets with high compatibility [33], and combining PDMS with conductive fabric [34], [35]. In this work, a copper foil was employed for the radiating element and the ground plane for the antenna prototype.

It should be mentioned that extensive studies were conducted to check the compatibility of copper foil with PDMS. In particular, in [25], a CP patch antenna which was totally encapsulated in a PDMS substrate where the durability and robustness of the antenna was reported. Copper foil was used for the patch and ground plane of the antenna. Robustness tests such as bending, temperature and wet proved that the antenna can maintain its performance even after deformation. The CP patch antenna has a broadband performance with a FBW of 21.5%. The proposed FSP antenna in this work is also designed using copper foil and is fully enclosed inside a PDMS substrate to provide robustness to the structure.

In the past, PDMS has also been used in applications involving molecular microchannel and biomolecular detection using microfluidic devices [36], [37]. PDMS has also been used recently for flexible antennas as well. In [38], an assessment of PDMS technology was presented with the use of a multiple-input-multiple-output (MIMO) antenna operating at 5.8 GHz for WLAN applications. The use of PDMS substrates for single frequency patch antennas has also been demonstrated in [39], [40].

IV. ANTENNA SYNTHESIS AND ANALYSIS

It is well known that the standard microstrip patch antenna has a resonant electrical length of about $\lambda/2$ and its electric-field is zero at the centre of the patch. Therefore, a shorting

TABLE 2. Dimensions of the three-layer FSP antenna.

Parameter	Value (mm)
L_1	32
L_2	32
L_3	38
$W_1 = W_2 = W_3$	40
h_1	5.0
h_2	2.2
h_3	12.7
y_p	5.0
d	1.0
Ground Plane	200×200
Ground Plane (thickness)	0.1

plate can be introduced at the centre of the patch, as well as the folding of the ground plane, without significantly affecting the resonant frequency and matching. Based on this miniaturization technique, a three-layer FSP antenna is designed and fabricated in this work. Electric-fields are also analyzed in detail to study the operating modes.

A. GEOMETRY OF THE FOLDED-SHORTED PATCH (FSP) ANTENNA

To design a FSP antenna, the ground plane and shorted patch can be folded twice defining a physical length of λ/12 defining the formation of the three-layered FSP. The three folded layers can have lengths: L_1, L_2 and L_3 as described in Fig. 3(a), and the total height of the conducting part of the antenna can be defined as $H = h_1 + h_2 + h_3$ where h_1, h_2 and h_3 are not equal. L_g characterizes the gap between the folded metallic layers and the metallic side wall, while h_3 defines the radiating slot for the dominant TM_{010} mode. d is the distance between layer 3 and air. Fig. 3(b) shows W_1, W_2 and W_3 which are the widths of the horizontal layers above the ground plane. Throughout the paper, length is denoted with L and width is denoted with W. Dimensions of the designed and optimized FSP antenna are also indicated in Table 2.

B. FABRICATION OF THE FOLDED-SHORTED PATCH (FSP) ANTENNA USING FLEXIBLE POLYDIMETHYLSILOXANE (PDMS)

The PDMS material used in this paper consists of two parts: polymer elastomer Sylgard 184 and its curing agent [41]. PDMS is initially in liquid form, and this polymer then hardens, is mixed and then cured by heating using its curing agent. Following this approach a multilayer PDMS implementation is able to deliver high robustness and flexibility for the proposed three-layer FSP.

The assembly process consists of five steps. First, the 1 mm top PDMS layer was produced (see Table 2 and Fig. 3). The Sylgard 184 silicone elastomer was mixed with its curing agent. Next, the gelatine PDMS layer was cured in an oven at 60°C for three hours. Once the PDMS hardened, in a second step a three-layered conducting element made of copper foil which is 0.035 mm thick was placed at the centre of the PDMS structure. This conducting element is the folded metallic layers which defines the FSP antenna as illustrated in Fig. 3(a). Then, in the third step, the 19 mm PDMS substrate was cured and processed again by following step 1 and then is left in an oven for hardening. At this stage the radiating element is completely embedded within PDMS. Finally, a 0.035 mm thick copper foil, which forms the ground plane was placed on the bottom of the structure. Each layer bonds to the adjacent layer in a natural way after hardening, without any glue or pre-preg.

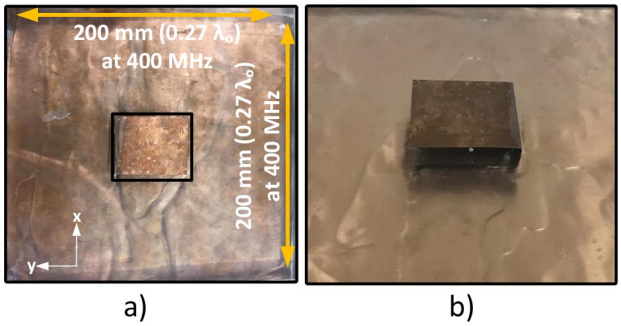

FIGURE 4. Fabricated and measured FSP antenna prototype for UHF and ISM bands communications: (a) top view and (b) perspective side view. The main radiating element is highlighted with (overlaid) solid black lines in (a).

C. FSP ANTENNA PROTOTYPE

The FSP antenna prototype was hand-made in a laboratory setting. The dimension of the fabricated antenna is $0.27\lambda_o \times 0.27\lambda_o \times 0.025\lambda_o$ at 400 MHz. The position of the shorting plates and structure dimensions were optimized in order to improve the matching, bandwidth, and antenna gain at the operating frequencies. Furthermore, the location of the feed was selected to achieve a good 50 Ω impedance matching. PDMS is used as the substrate and its cover such that the antenna is fully embedded as shown in Figs. 3 and 4. The overall thickness of the PDMS substrate is slightly larger than the FSP for two reasons: it improves impedance FBW [42] and because it is developed for the noted wearable application providing robustness and a stronger mechanical support for the antenna structure when placed on a user and when considering a potentially harsh operating environment.

The ground plane is also larger than the antenna itself because the FSP is meant to be positioned in a bulletproof jacket which has inbuilt metal. Having such a large ground plane creates a simple isolation mechanism and with low cross-polarization levels at the dominant mode. Nowadays, on average the mass of the bulletproof jacket is approximately 15 kg and the prototyped antenna mass is only about 0.9 kg. This potentially is not a major concern for military and emergency response teams since their gear can total up to 23 kg.

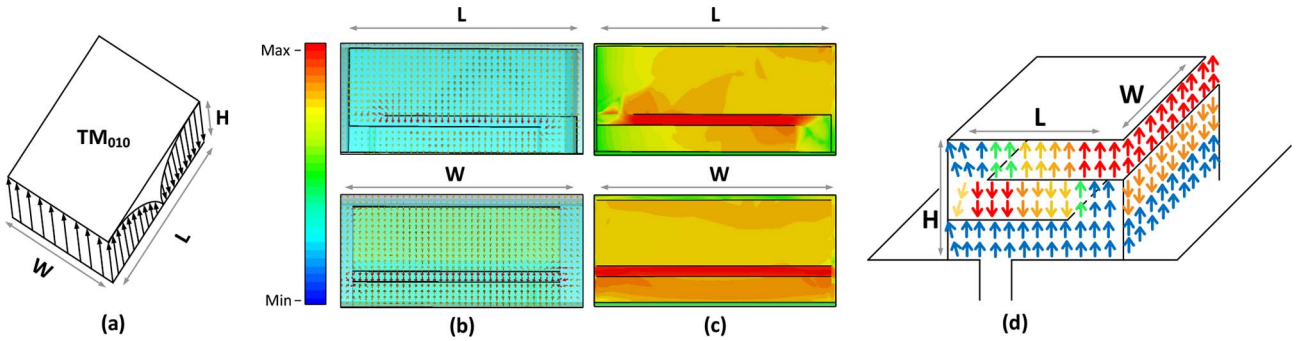

FIGURE 5. (a) Illustration of the electric-field for the TM_{010} mode of the conventional patch antenna. (b) The CST simulated electric-field (V/m) within the three-layer FSP antenna at 400 MHz. The colour bar defines the strength of the electric-field in the different layers. (c) An amplitude representation is shown for the TM_{010} dominant mode of the FSP antenna. (d) Sketched vector electric-field pattern of the TM_{010} mode for the FSP antenna. The arrows indicate the phase and magnitude of the current along the length (L) and width (W) of the structure.

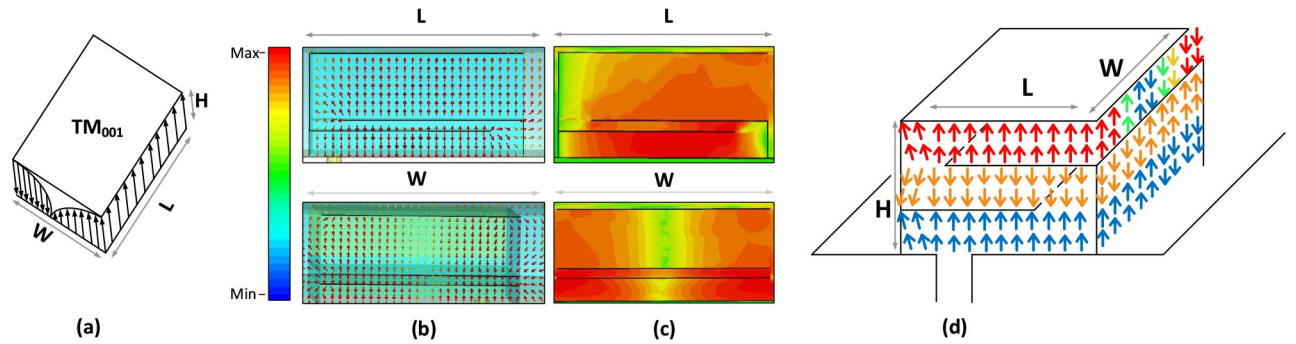

FIGURE 6. (a) Illustration of the electric-field for the conventional patch antenna for the higher order TM_{001} mode. (b) The simulated vector electric-field (V/m) within the three-layer FSP antenna at 2.4 GHz. (c) An amplitude representation is shown for the TM_{001} higher order mode of the FSP antenna (d) Sketched vector electric-field pattern of the TM_{001} mode for the FSP antenna. The arrows indicate the phase and magnitude of the current along the length (L) and width (W) of the structure.

D. TM_{010} AND TM_{001} MODE COMPARISON OF THE THREE-LAYER FSP ANTENNA AND THE CONVENTIONAL PATCH

To characterize the modes for the FSP, the resonant frequency equations such as $f_{010} \approx 1/4L\sqrt{\mu\epsilon}$ and $f_{001} \approx 1/4W\sqrt{\mu\epsilon}$, can be used starting from [28], [42] for the conventional patch. Here L is the length of the radiating element, W is the width of the radiating element, μ and ϵ are the permeability and permittivity of the substrate, respectively (see Fig. 3). These equations should also satisfy the conditions such that $L > W > H$ for the TM_{010} mode and $L > W > L/2$ for the TM_{001} mode [28], [42]. Here, $H = h_1 + h_2 + h_3$ refers to the thickness of the antenna as in Fig. 3 and Table 2.

The proposed FSP antenna operates at the TM_{010} and TM_{001} modes and in the next section, a comparative analysis using the cavity model [28] is provided. To the best knowledge of the authors' no similar modal analysis has been applied to the FSP structures.

E. ELECTRIC-FIELD DISTRIBUTION

The field configurations for the conventional patch and the FSP cavity models are compared in Figs. 5 and 6. Based on CST simulations, it is observed that the electric fields of the FSP antenna are concentrated near the open edges. Figure 5(a-d) shows the electric-field distribution within the substrate and the radiating element and the ground plane. For the TM_{010} mode the fields undergo a phase reversal along the length (L) of the patch and the FSP but they are uniform along the width (W). This uniform pattern along W contributes significantly to the radiation. The phase reversal along L is important for the antenna to generate a broadside radiation pattern in the far-field [28]. Also, the FSP operating at 400 MHz has a similar electric-field pattern to the dominant TM_{010} mode for the conventional patch.

For the higher order TM_{001} mode, the electric-field pattern is uniform along L of the patch and the FSP, and the fields are in phase reversal along W as shown in Fig. 6(a-d). For the FSP operating at 2.4 GHz, the electric-field pattern is similar to the field at the TM_{001} mode. The three-layer FSP proposed in this paper operates at the TM_{010} and TM_{001} modes offering broadside radiation and without any slot loading in the top aperture as done in [24] and [27] which can potentially alter the BW and introduce a beam squint.

1) FIELDS RADIATED BY THE TM_{010} MODE

From the equivalence principle, it is known that each slot radiates the same field and can be modelled as a magnetic dipole with current density $M_s = -2n \times E_a$ where n and E_a are the unit normal vector and electric-field at the slots, respectively. The equivalent magnetic current densities along the two slots, each of width W and height H, are both of the same magnitude and same phase [28]. Therefore, these two

slots form a two-element array. The fields generated by these two sources will constructively interfere in a direction normal to the patch and ground plane, forming a broadside pattern in the far-field. Considering the operation of the single-layer patch at the TM_{010} mode, the radiated field and directivity by these two slots can be defined (based on [28], Ch. 14, eqs. (14-45)-(14-46)).

On the other hand, the FSP antenna investigated in this work has three electric and three magnetic walls. Hence, fields radiated by the FSP antenna is through a single slot. In order to analyze these fields at the top layer, a similar procedure is followed as mentioned above for the conventional patch. For the FSP, the equivalent magnetic current densities are concentrated along the single slot on the top layer. Therefore, the electric-fields radiated by a single slot in the far-field using an equivalent current can be shown to be:

$$E_\phi = \frac{kHWE_o e^{-jk_o r}}{\pi r}\left\{\sin\theta \frac{\sin(X)}{X}\frac{\sin(Z)}{Z}\right\}$$
$$\text{where } X = \frac{kH}{2}\sin\theta\cos\phi, Z = \frac{kW}{2}\sin\theta,$$
$$k = k_o \times \sqrt{\varepsilon_r}. \quad (1)$$

The E- and H-plane pattern using the cavity model for the TM_{010} mode has been plotted by Eq. (1) using MATLAB and compared with CST simulations for the FSP and the patch antenna at 400 MHz (results not shown for brevity) considering an air substrate; i.e., $\varepsilon_r = 1.00057$. These theoretical and CST simulated beam patterns were also analyzed for $\epsilon_r = 2.8$ (PDMS).

2) FIELDS RADIATED BY THE HIGHER-ORDER TM_{001} MODE

Similar to the dominant TM_{010} mode, the conventional patch antenna and the FSP were analyzed using the cavity model and simulated using CST for the TM_{001} mode. Both consider an infinite ground plane and where the dielectric material is only defined by the dimensions of the single radiating element. For the TM_{001} mode, the magnetic current densities have the same magnitude and the same phase along the two slots (L and H from Fig. 6) of the patch and the FSP. Therefore, these two slots form the two-element array with the sources of the same magnitude and phase separated by W. Due to the change in the radiating aperture from W (TM_{010} mode) to L (TM_{001} mode), a change in polarization can be observed.

The electric-field radiated by the slots for the higher order TM_{001} mode follows the procedure outlined above for the dominant TM_{010} mode. The total electric-field for the patch and the FSP are:

$$E_\phi = \frac{kHLE_o e^{-jkr}}{\pi r}\left\{\cos\theta\sin\phi\frac{\sin(X)}{X}\frac{\sin(Y)}{Y}\right\}$$
$$\times \cos\left(\frac{kW}{2}\cos\theta\right)$$

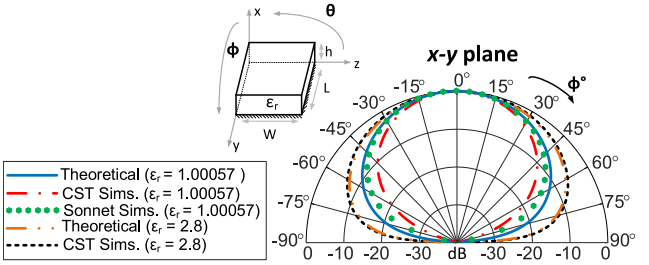

FIGURE 7. Beam pattern for the conventional patch antenna in the *x-y* plane for the higher order mode (TM_{001}). The theoretical beam patterns were plotted using Eq. (2). These cavity model calculations were compared with Sonnet and CST simulations ($h = H$).

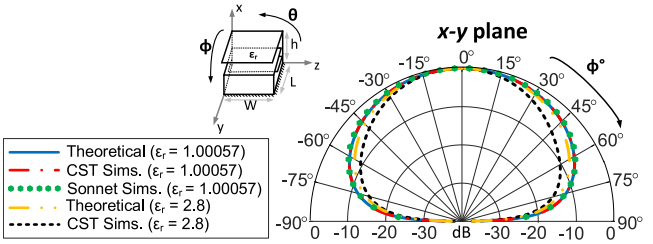

FIGURE 8. Beam pattern for the FSP antenna in the *x-y* plane for the TM_{001} higher order mode. The theoretical beam pattern was plotted using Eq. (2) by the cavity model ($h = H$).

and

$$E_\theta = \frac{kHLE_o e^{-jkr}}{\pi r}\left\{\cos\phi\frac{\sin(X)}{X}\frac{\sin(Y)}{Y}\right\}$$
$$\times \cos\left(\frac{kW}{2}\cos\theta\right)$$
$$\text{where } X = \frac{kH}{2}\sin\theta\cos\phi, Y = \frac{kL_e}{2}\sin\theta\sin\phi,$$
$$k = k_o \times \sqrt{\epsilon_r}. \quad (2)$$

For both antennas, the x-y plane ($\theta = 90°, 0° \geq \phi \geq 90°$ and $270° \geq \phi \geq 360°$) is the principal E-plane while the H-plane is the x-z plane ($\phi = 0°, 0° \geq \theta \geq 180°$). Figs. 7 and 8 report the beam pattern for the conventional patch and the FSP antenna at the TM_{001} mode, respectively. The numerically determined results were compared with the commercial software packages CST and Sonnet. The FSP and the patch antenna was designed using air as a substrate with an infinite ground plane. A good agreement between the theoretical and simulated beam patterns can be observed.

F. BROADSIDE DIRECTIVITY FOR THE TM_{010} AND TM_{001} MODES

Directivity equations developed from the procedure mentioned in [28] for the dominant mode of the conventional patch are now extended to the three-layer FSP and the TM_{001} mode. Due to the existence of the two slots, an array factor can be used in the development. The general equation for the directivity of a patch antenna for the TM_{010} mode is provided in ([28], Ch. 14, eqs. (14-55)-(14-56)).

For the FSP, at the TM_{010} mode the fields are radiated from a single slot. Hence, the directivity for the FSP can

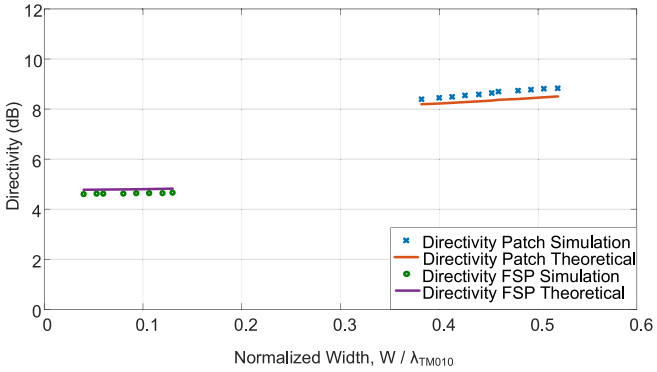

FIGURE 9. Numerically calculated directivity for the conventional patch antenna and the FSP (Eq. (3)) at the TM_{010} mode. Full-wave CST simulations of the conventional patch antenna and the three-layer FSP antenna are in close agreement with numerically derived directivity values. Both antennas are probe fed with air as a substrate between the metallic layers. Results are compared when the width is normalized by the wavelength considering the TM_{010} mode.

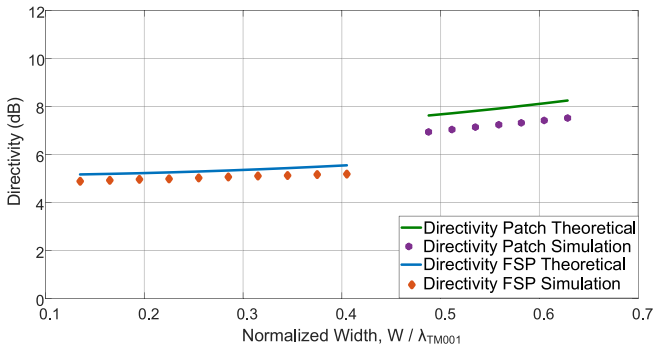

FIGURE 10. Numerically calculated directivity for the conventional patch antenna and the FSP antenna (Eq. (4)) at the TM_{001} higher order mode. Full-wave simulations of the conventional patch antenna and the three-layer FSP antenna are in close agreement. Both antennas are probe fed with air as a substrate between the metallic layers.

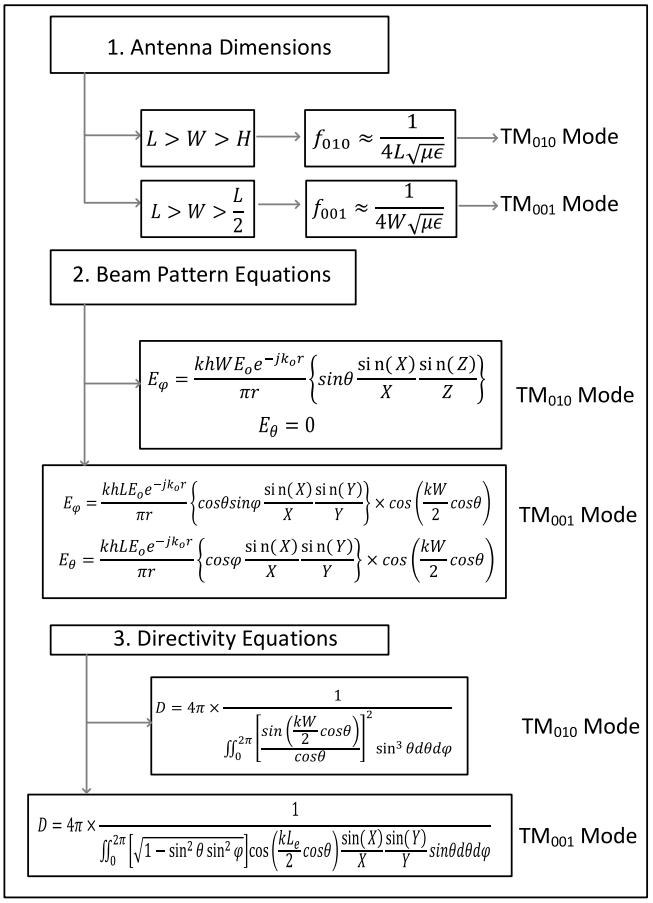

FIGURE 11. Diagram summarizing the step-by-step design procedure and modelling approach for the FSP ensuring the TM_{010} and TM_{001} modes. Step 1 shows the dimension needed (see Section II, page 4). From step 2 the beam pattern can be found (see Eqs. (1) and (2), here $h = H$). Finally, step 3 shows the equations that can be used to calculate the peak directivity of the FSP (see Eqs. (3) and (4)).

be derived using the procedure outlined in ([28], Ch. 14, eqs. (14-55)-(14-56)) for the conventional patch but without an array factor term:

$$D = 4\pi \times \frac{1}{\int_0^{2\pi}\int_0^{\pi}\left[\dfrac{\sin\left(\frac{kW}{2}\cos\theta\right)}{\cos\theta}\right]^2 \sin^3\theta d\theta d\phi} \quad (3)$$

The theoretically determined directivity for both the conventional patch antenna and the FSP considering an air dielectric ($\varepsilon_r = 1.00057$) have been plotted using MATLAB and compared to full-wave CST simulations in Fig. 9. It can be observed that the directivity of the FSP is reduced by up to 4 dB when compared with the conventional patch antenna. Similarly, using the aforementioned procedure to derive the directivity for the TM_{010} mode, an expression for the directivity for the TM_{001} mode can be also be obtained (see Eq. (4)). In Fig. 10 a comparison of the directivity for the FSP and the conventional patch antenna at the TM_{001} mode is shown considering an air dielectric.

$$D = 4\pi \times \frac{1}{\int_0^{2\pi}\int_0^{\pi}[\sqrt{1-\sin^2\theta\sin^2\phi}]AUV\sin\theta d\theta d\phi}$$
$$\text{where } A = \cos\left(\frac{kL_e}{2}\cos\theta\right),\quad U = \frac{\sin(X)}{X},\quad V = \frac{\sin(Y)}{Y}. \quad (4)$$

G. SUMMARY OF THE DEVELOPED ANALYSIS AND DESIGN APPROACH

In this work, a complete and newly developed analysis for the design of the FSP has been reported along with simple design equations which follow the cavity model. These findings can allow the antenna designer to predict the beam pattern shape and peak directivity values. Fig. 11 shows a summarized design flow diagram starting from the dimensions needed to calculate the peak directivity of the FSP. These design equations help to ensure operation of the relevant TM modes. Also, once the modes of the antenna have been achieved, the pattern of the antenna can be estimated using Eqs. (1) and (2) to ensure an omni-directional-like beam pattern with no nulls. It should also be mentioned that the beam patterns

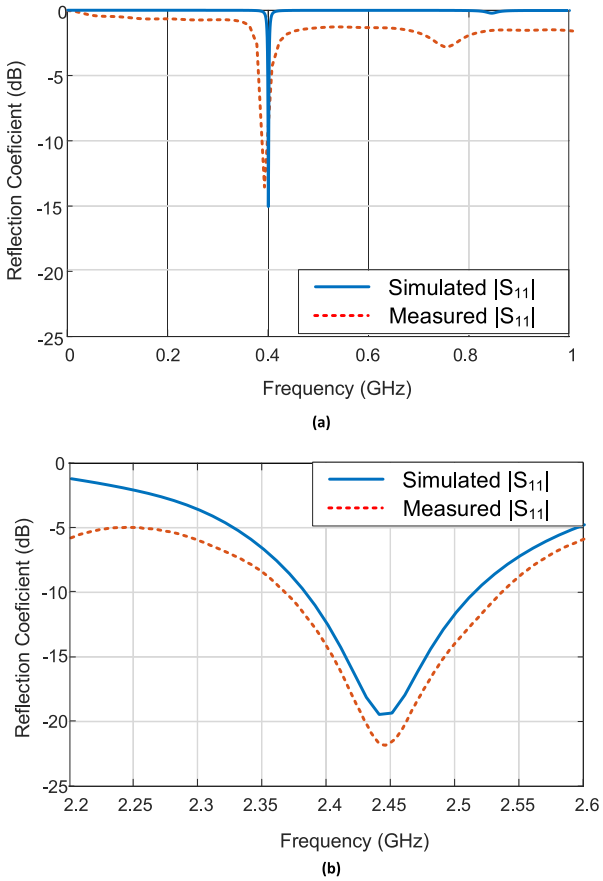

FIGURE 12. Measured and simulated $|S_{11}|$ of the proposed FSP antenna prototype shown in Fig. 4 and compared to CST simulations. (a) The structure accepts power at about 400 MHz (UHF band) where $|S_{11}|$ is less than −10 dB. (b) At 2.45 GHz (ISM band) the $|S_{11}|$ is less than −10 dB and −20 dB for the simulation and measurement, respectively.

of other operating modes (such as the TM_{020} or the TM_{030} mode) can also be derived using the procedure mentioned in [28]. Likewise, the peak directivity of the FSP antenna can also be calculated using Eqs. (3) and (4).

V. ANTENNA MEASUREMENTS AND DISCUSSIONS

A. REFLECTION COEFFICIENT OF THE FSP ANTENNA PROTOTYPE

The $|S_{11}|$ results in Fig. 12 (a) and (b) suggests that the FSP antenna operates at 400 MHz and at 2.45 GHz, respectively. Both the dominant TM_{010} mode and the higher order TM_{001} mode corresponds to a good matching condition ($|S_{11}| \leq -10$ dB) at about 400 MHz and 2.45 GHz, respectively, enabling multi-band operation. Moreover, at 400 MHz the FSP antenna is acting as a beacon and does not require a large BW; i.e., a 13 MHz of BW is observed at the dominant mode for both simulations and measurements. Also, the large ground plane of the antenna helps to improve radiation away from the body and a BW of approximately 180 MHz is observed at the higher order mode for the centre frequency at 2.45 GHz.

Due to the folding technique, the BW at 400 MHz is relatively narrow but also due to the compactness of the

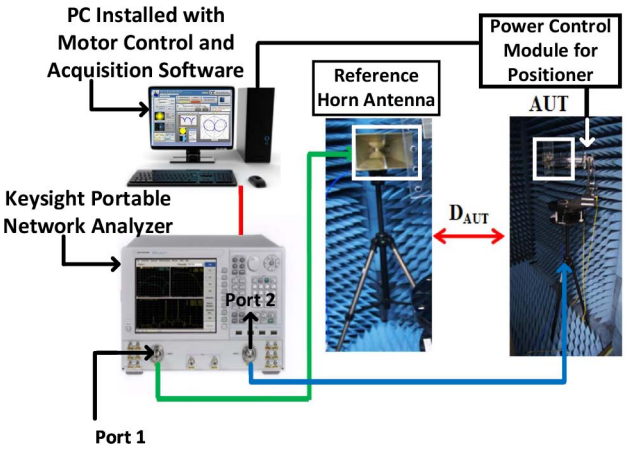

FIGURE 13. Illustration of the radiation pattern measurement system inside the anechoic chamber at Heriot-Watt University.

structure. However, by increasing the separation between metallic layers the BW can be increased while maintaining a low profile for the FSP [22]. It should also be mentioned that a minor discrepancy can be observed between the measured and simulated results mainly due to the presence of air bubbles (or air gap) in the fabricated FSP structure as well as slight disagreements between the modelled and the actual relative dielectric constant and loss tangent for the PDMS material, and probe position. All these factors were taken into consideration during antenna design and optimization. Nonetheless, the $|S_{11}|$ is still below −10 dB at 400 MHz and at 2.45 GHz.

B. RADIATION PATTERN

The radiation pattern measurements took place inside an anechoic chamber using a Keysight vector network analyzer (VNA) available at Heriot-Watt University and were based on a far-field antenna measurement. Fig. 13 shows the setup. Port 1 of the VNA is connected to the horn antenna defined as the transmitting or reference antenna. Port 2 of the VNA is connected to the antenna under test (AUT) as the receiver. The VNA is set to acquire S_{21} measuring the radiation pattern from Port 1 to Port 2, while the VNA is linked to the computer via USB cable. The AUT and horn antenna are separated with a distance of D_{AUT}. The AUT is rotated 360° in a single plane during the polar radiation pattern measurement.

The *x-z* plane and the *x-y* plane radiation patterns at 400 MHz are shown in Fig. 14 for the dual-band antenna operating at the TM_{010} mode. The simulated and measured peak cross-polarization levels are at least 20 dB below the main co-pol maximum at broadside. Similarly, at 2.45 GHz (TM_{001} mode), the radiation patterns in the *x-z* and *y-z* planes are shown in Fig. 15. It is worth noting that there is a change in the polarization in comparison with the dominant TM_{010} mode.

At 2.45 GHz when the FSP antenna operates in the TM_{001} mode, the beam pattern is abrupt and directive. This is due

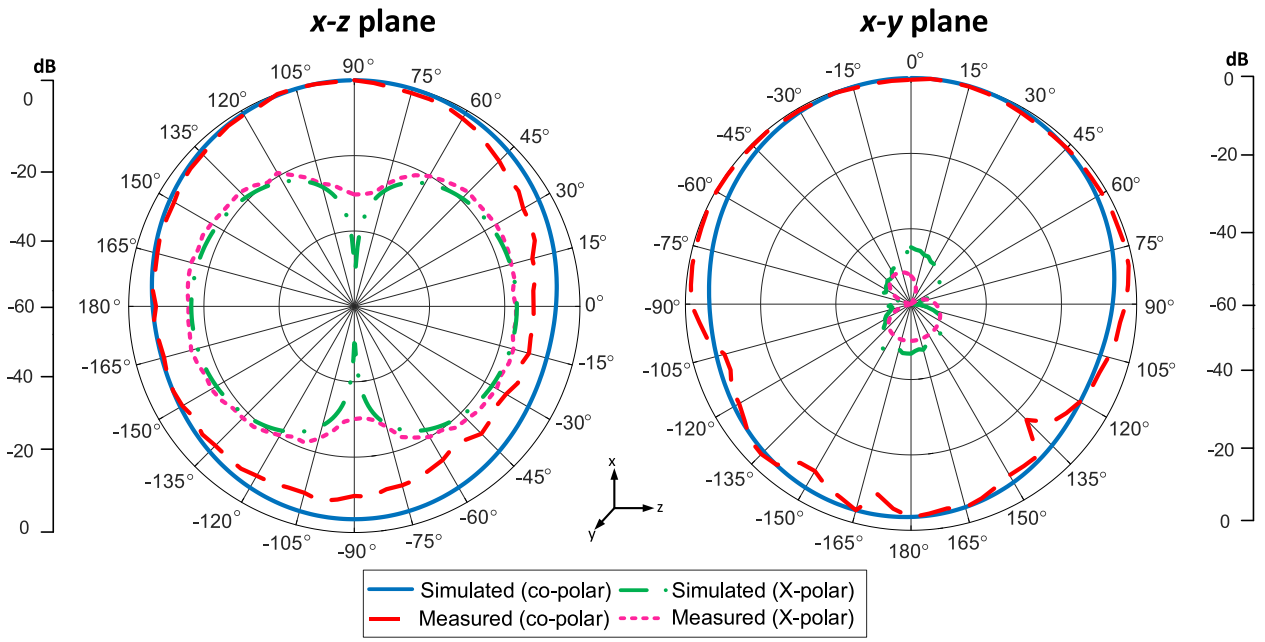

FIGURE 14. Three layer FSP antenna where beam patterns in both the *x-z* and *y-z* planes are shown at 400 MHz for the dominant TM_{010} mode. Cross polarization levels are also shown and are more than 20 dB below the main co-polarized maximum at broadside.

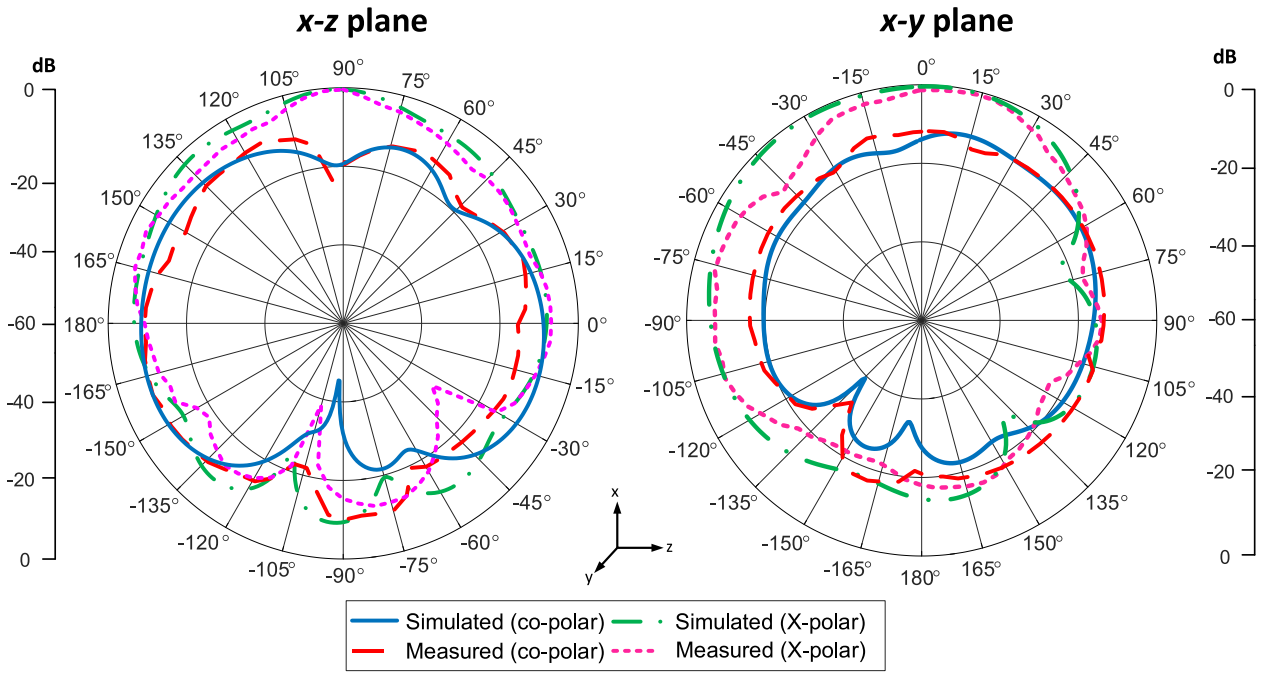

FIGURE 15. Three layer FSP antenna where beam patterns in both the *x-z* and *y-z* planes are shown at 2.4 GHz for the higher order TM_{001} mode. It should be mentioned that the co-polar and cross-polar field values are defined by the fundamental TM_{001} mode.

to the equal substrate and ground plane size. On the other hand, the broadside pattern shown in recent FSP antennas (previously reported designs) operated by the TM_{030} mode [24], [27]. This is due to the following reasons: (a) the substrate used is truncated at the edge of the radiating element or has no substrate that limits the generation of magnetic currents at the edges, resulting in low electric-fields between the radiating element and ground plane, and (b) introduction of slots that minimizes the effect of grating lobes ensuring a single beam with one dominant main lobe and not like the multi-beam pattern plot in Fig. 2 for the TM_{030} mode.

The peak realized gain of the antenna measured in free space is 1.40 dBi and 3.20 dBi at 400 MHz and 2.4 GHz, respectively. Since the FSP antenna is designed for wearable applications, the specific absorption rate (SAR) is another

TABLE 3. Widths variation for layers 2 and 3 for constant TM_{001} mode.

W_3 (mm)	ΔW_2 (mm)	TM_{010} Mode Best Matching (MHz)	$\|S_{11}\|$ [dB]	TM_{001} Mode Best Matching (GHz)	$\|S_{11}\|$ [dB]
40	38	404.6	-12.03	2.40	-13.20
40	39	402.2	-13.90	2.40	-14.73
40	40	401.0	-12.82	2.40	-15.03
40	41	399.0	-11.55	2.40	-16.91
40	42	398.0	-13.30	2.40	-17.43

TABLE 4. Length variation for layer 3 for constant TM_{010} mode.

L_3 (mm)	ΔL_3 (mm)	TM_{010} Mode Best Matching (MHz)	$\|S_{11}\|$ [dB]	TM_{001} Mode Best Matching (GHz)	$\|S_{11}\|$ [dB]
40	0	401.0	-16.95	2.46	-21.55
41	1	401.0	-14.45	2.39	-21.20
42	2	401.0	-12.80	2.35	-21.66
43	3	401.0	-12.15	2.30	-21.16

important parameter to consider. For example, the values of SAR were simulated to be 0.14 W/kg and 1.06 W/kg at 400 MHz and 2.45 GHz, respectively, when considering a human phantom. Also, these SAR values are much lower than the maximum limit set by the Council of the European Union (2.0 W/kg). The simulated realized gain of the FSP antenna when placed on a human body model at 400 MHz and 2.4 GHz are 1.37 dBi and 3.10 dBi, respectively. This suggests that the realized gain is not significantly affected by the human body.

The radiation efficiency of the FSP antenna in free space is 54% and 70% at 400 MHz and 2.4 GHz, respectively, and when the antenna is on human body it is 50% and 65%. The antenna could be considered to have a low efficiency and realized gain at the dominant mode but this is not a major concern since the FSP is acting as a beacon antenna requiring low data rates. At 2.4 GHz, the realized gain and efficiency achieved is suitable for WiFi communications as similar efficiency and gain values were reported for wearable antennas. For example, in [43] and [44] wearable antennas were designed at 2.45 GHz and the radiation efficiency when antenna is placed on body was reported to be 22% and 26%, respectively.

C. TUNING PROCEDURE

A tuning procedure is also reported here to optimize antenna matching and radiation performance at the operational frequency. This study is important to facilitate the understanding of the relevant design parameters needed to tune within the FSP for engineers interested to replicate this work, quickly change the resonant frequency or introduce some active elements. For example, should TM_{001} operation be required at 2.4 GHz while antenna operation needs to be varied from about 400 MHz to another frequency. The width W_2 can be altered by ΔW_2 with a 5 % variation from its original size and keeping W_3 constant. In Table 3, it can be observed that the resonant frequency of the higher order mode is constant (at 2.4 GHz) but the resonant frequency of the dominant mode is tuned around 400 MHz.

A similar procedure was performed for L_3 which was altered by ΔL_3. It can be observed that the dominant mode frequency is constant but the higher order mode frequency changes. These variations are reported in Table 4. Hence, the tuning procedure suggests that the higher or lower frequency can be controlled independently while keeping one of the operating frequencies constant.

VI. CONCLUSION

This paper presented the design, fabrication and measurement of a dual-band three-layer FSP antenna operational at the TM_{010} (400 MHz) and the TM_{001} (2.4 GHz) modes. An analysis of the different modes was performed and the far-field beam patterns were numerically determined using the cavity model. Results are in agreement with values obtained from full-wave simulations using CST. In addition, directivity equations for the conventional patch and the proposed three-layer FSP have been derived and verified considering the TM_{010} and the TM_{001} modes.

The major dimensions of the FSP prototypes are $0.27\lambda_o \times 0.27\lambda_o \times 0.025\lambda_o$ based on the lower design frequency of 400 MHz. Also, the reported measurements are generally in close agreement with the simulated results. Radiation is at broadside for 400 MHz and 2.4 GHz and maximum realized gain values of 1.4 and 3.0 dBi are observed, respectively. For the antenna to operate for Wi-Fi applications, it is recommended to have $|S_{11}|$ below -25 dB. This can be made possible by optimizing the width of the folded elements and probe position. The FBW of the antenna can be improved by increasing the thickness of the FSP antenna or by introducing slots as mentioned in [24] but this might increase the overall size of the antenna and its design complexity which might not be suitable. The radiation performance of the developed PDMS-based and low-profile FSP, when operating both in free-space and when placed on a human phantom, suggest that the antenna can be suitable for wearable applications such as military search and rescue operation and emergency services where antenna robustness is important.

ACKNOWLEDGMENT

The authors would like to indicate that the work is only the authors' views, and that the Horizon 2020 Agency is not responsible for any information contained in the paper.

REFERENCES

[1] J. Farringdon, A. J. Moore, N. Tilbury, J. Church, and P. D. Biemond, "Wearable sensor badge and sensor jacket for context awareness," in *Dig. Papers 3rd Int. Symp. Wearable Comput.*, San Francisco, CA, USA, Oct. 1999, pp. 107–113.

[2] E. J. Lind *et al.*, "A sensate liner for personnel monitoring applications," in *Dig. Papers 1st Int. Symp. Wearable Comput.*, Cambridge, MA, USA, Oct. 1997, pp. 98–105.

[3] S. J. Schwartz and A. Pentland, "The smart vest: Towards a next generation wearable computing platform," Dept. Perceptual Comput. Sec., MIT Media Lab., Cambridge, MA, USA, Rep. 504, 1999.

[4] B. Sanz-Izquierdo, J. A. Miller, J. C. Batchelor, and M. I. Sobhy, "Dual-band wearable metallic button antennas and transmission in body area networks," *IET Microw. Antennas Propag.*, vol. 4, no. 2, pp. 182–190, Feb. 2010.

[5] G. Li, G. Gao, J. Bao, B. Yi, C. Song, and L.-A. Bian, "A watch strap antenna for the applications of wearable systems," *IEEE Access*, vol. 5, pp. 10332–10338, 2017.

[6] G. Monti, L. Corchia, E. D. Benedetto, and L. Tarricone, "Wearable logo-antenna for GPS–GSM-based tracking systems," *IET Microw. Antennas Propag.*, vol. 10, no. 12, pp. 1332–1338, Sep. 2016.

[7] N. H. M. Rais, P. J. Soh, F. Malek, S. Ahmad, N. B. M. Hashim, and P. S. Hall, "A review of wearable antenna," in *Proc. Loughborough Antennas Propag. Conf.*, Loughborough, U.K., Nov. 2009, pp. 225–228.

[8] J. Matthews and G. Pettitt, "Development of flexible, wearable antennas," in *Proc. IEEE 3rd Eur. Conf. Antennas Propag.*, Berlin, Germany, 2009, pp. 273–277.

[9] J. Lilja *et al.*, "Body-worn antennas making a splash: Lifejacket-integrated antennas for global search and rescue satellite system," *IEEE Antennas Propag. Mag.*, vol. 55, no. 2, pp. 324–341, Apr. 2013.

[10] S. Genovesi, F. Costa, F. Fanciulli, and A. Monorchio, "Wearable inkjet-printed wideband antenna by using miniaturized AMC for sub-GHz applications," *IEEE Antennas Wireless Propag. Lett.*, vol. 15, pp. 1927–1930, 2016, doi: 10.1109/LAWP.2015.2513962.

[11] S. Zhu and R. Langley, "Dual-band wearable textile antenna on an EBG substrate," *IEEE Trans. Antennas Propag.*, vol. 57, no. 4, pp. 926–935, Apr. 2009.

[12] H. Lee, J. Tak, and J. Choi, "Wearable antenna integrated into military berets for indoor/outdoor positioning system," *IEEE Antennas Wireless Propag. Lett.*, vol. 16, pp. 1919–1922, 2017, doi: 10.1109/LAWP.2017.2688400.

[13] J. R. James, A. J. Schuler, and R. F. Binham, "Reduction of antenna dimensions by dielectric loading," *Electron. Lett.*, vol. 10, no. 13, pp. 263–265, Jun. 1974.

[14] T. Lo, C. Ho, Y. Hwang, E. Lam, and B. Lee, "Miniature aperture-coupled microstrip antenna of very high permittivity," *Electron. Lett.*, vol. 33, no. 1, pp. 9–10, Jan. 1997.

[15] J. S. Colburn and Y. Rahmat-Samii, "Patch antennas on externally perforated high dielectric constant substrates," *IEEE Trans. Antennas Propag.*, vol. 47, no. 12, pp. 1785–1794, Dec. 1999.

[16] W.-S. Chen, "Single-feed dual-frequency rectangular microstrip antenna with square slot," *Electron. Lett.*, vol. 34, no. 3, pp. 231–232, Feb. 1998.

[17] K.-P. Yang and K.-L. Wong, "Inclined-slot-coupled compact dual-frequency microstrip antenna with cross-slot," *Electron. Lett.*, vol. 34, no. 4, pp. 321–322, Feb. 1998.

[18] K.-L. Wong and K.-P. Yang, "Compact dual-frequency microstrip antenna with a pair of bent slots," *Electron. Lett.*, vol. 34, no. 3, pp. 225–226, Feb. 1998.

[19] J. L. Volakis, C.-C. Chen, and K. Fujimoto, *Small Antennas: Miniaturization Techniques & Applications*, vol. 1. New York, NY, USA: McGraw-Hill, 2010.

[20] Z. Li and Y. Rahmat-Samii, "Optimization of PIFA-IFA combination in handset antenna designs," *IEEE Trans. Antennas Propag.*, vol. 53, no. 5, pp. 1770–1778, May 2005.

[21] R. Li, G. DeJean, M. M. Tentzeris, and J. Laskar, "Development and analysis of a folded shorted-patch antenna with reduced size," *IEEE Trans. Antennas Propag.*, vol. 52, no. 2, pp. 555–562, Feb. 2004.

[22] S. K. Podilchak *et al.*, "A compact circularly polarized antenna using an array of folded-shorted patches," *IEEE Trans. Antennas Propag.*, vol. 61, no. 9, pp. 4861–4867, Sep. 2013.

[23] A. Holub and M. Polivka, "A novel microstrip patch antenna miniaturization technique: A meanderly folded shorted-patch antenna," in *Proc. 14th Conf. Microw. Techn.*, Prague, Czechia, Apr. 2008, pp. 1–4.

[24] K. L. Lau, K. C. Kong, and K. M. Luk, "A miniature folded shorted patch antenna for dual-band operation," *IEEE Trans. Antennas Propag.*, vol. 55, no. 8, pp. 2391–2398, Aug. 2007.

[25] R. Joshi, C. Constantinides, S. K. Podilchak, M. N. Ramli, H. Lago, and P. J. Soh, "Robust and compact PDMS antennas for search and rescue operations and emergency communications," in *Proc. 12th Eur. Conf. Antennas Propag. (EuCAP 2018)*, London, U.K., Apr. 2018, pp. 1–5.

[26] R. Joshi and P. J. Soh, "Dual-band folded-shorted patch antenna for military search and rescue operations and emergency communications," in *Proc. 18th Int. Symp. Antenna Technol. Appl. Electromagn. (ANTEM)*, Waterloo, ON, Canada, Aug. 2018, pp. 1–2.

[27] D. E. Brocker, Z. H. Jiang, M. D. Gregory, and D. H. Werner, "Miniaturized dual-band folded patch antenna with independent band control utilizing an interdigitated slot loading," *IEEE Trans. Antennas Propag.*, vol. 65, no. 1, pp. 380–384, Jan. 2017.

[28] C. A. Balanis, *Antenna Theory: Analysis and Design*. Hoboken, NJ, USA: Wiley, 2016.

[29] S. Maci and G. B. Gentili, "Dual-frequency patch antennas," *IEEE Antennas Propag. Mag.*, vol. 39, no. 6, pp. 13–20, Dec. 1997.

[30] D. M. Pozar, *Microwave Engineering*, 4th ed. Hoboken, NJ, USA: Wiley, 2012.

[31] J. Trajkovikj and J.-F. Zürcher, and A. K. Skrivervik, "PDMS, a robust casing for flexible W-BAN antennas [EurAAP Corner]," *IEEE Antennas Propag. Mag.*, vol. 55, no. 5, pp. 287–297, Oct. 2013.

[32] A. C. Kuo, "Poly (dimethylsiloxane)," in *Polymer Data Handbook*. New York, NY, USA: Oxford Univ. Press, 1999, pp. 411–435.

[33] Y. Zhou, Y. Bayram, F. Du, L. Dai, and J. L. Volakis, "Polymer-carbon nanotube sheets for conformal load bearing antennas," *IEEE Trans. Antennas Propag.*, vol. 58, no. 7, pp. 2169–2175, Jul. 2010.

[34] R. B. V. B. Simorangkir, Y. Yang, R. M. Hashmi, T. Björninen, K. P. Esselle, and L. Ukkonen, "Polydimethylsiloxane-embedded conductive fabric: Characterization and application for realization of robust passive and active flexible wearable antennas," *IEEE Access*, vol. 6, pp. 48102–48112, 2018.

[35] A. Kiourti and J. L. Volakis, "Stretchable and flexible e-fiber wire antennas embedded in polymer," *IEEE Antennas Wireless Propag. Lett.*, vol. 13, pp. 1381–1384, 2014, doi: 10.1109/LAWP.2014.2339636.

[36] T. Fujii, "PDMS-based microfluidic devices for biomedical applications," *Microelectron. Eng.*, vols. 61–62, pp. 907–914, Jul. 2002.

[37] J. Zhou, A. V. Ellis, and N. H. Voelcker, "Recent developments in PDMS surface modification for microfluidic devices," *Electrophoresis*, vol. 31, no. 1, pp. 2–16, 2010.

[38] A. S. M. Alqadami, M. F. Jamlos, P. J. Soh, and G. A. E. Vandenbosch, "Assessment of PDMS technology in a MIMO antenna array," *IEEE Antennas Wireless Propag. Lett.*, vol. 15, pp. 1939–1942, 2016, doi: 10.1109/LAWP.2015.2513960.

[39] N. Tiercelin, P. Coquet, R. Sauleau, V. Senez, and H. Fujita, "Polydimethylsiloxane membranes for millimeter-wave planar ultra flexible antennas," *J. Micromech. Microeng.*, vol. 16, no. 11, p. 2389, 2006.

[40] C.-P. Lin, C.-H. Chang, Y. T. Cheng, and C. F. Jou, "Development of a flexible SU-8/PDMS-based antenna," *IEEE Antennas Wireless Propag. Lett.*, vol. 10, pp. 1108–1111, 2011, doi: 10.1109/LAWP.2011.2170398.

[41] D. Corning, "SYLGARD 184 silicone elastomer," Data Sheet, Dow Chem. Company, Midland, MI, USA, 2017.

[42] R. Garg, P. Bhartia, I. J. Bahl, and A. Ittipiboon, *Microstrip Antenna Design Handbook*. Boston, MA, USA: Artech House, 2001.

[43] A. Ruaro and J. Thaysen and K. B. Jakobsen, "Wearable shell antenna for 2.4 GHz hearing instruments," *IEEE Trans. Antennas Propag.*, vol. 64, no. 6, pp. 2127–2135, Jun. 2016.

[44] S. Su and Y. Hsieh, "Integrated metal-frame antenna for smartwatch wearable device," *IEEE Trans. Antennas Propag.*, vol. 63, no. 7, pp. 3301–3305, Jul. 2015.

RAHIL JOSHI was born in India. He received the B.E. degree (Hons.) in electronics and communication engineering from the Birla Institute of Technology and Sciences, Pilani, in 2014, and the M.Sc. degree in communication and signal processing from Newcastle University, U.K., in 2015. He is currently pursuing the Ph.D. degree in electrical engineering with specialization in RF and microwave engineering with the University of Edinburgh and Heriot-Watt University, Edinburgh, U.K.

His current research interests include design and analysis of wearable antennas for various applications, compact antennas, flexible transmission lines, wireless power transfer and software defined radios. In 2017, he received a research excellence award from Heriot-Watt University. He has been an Associate Fellow for Higher Education Academy, U.K., since 2017.

SYMON K. PODILCHAK (Member, IEEE) received the B.A.Sc. degree in engineering science from the University of Toronto, Toronto, ON, Canada, in 2005, and the M.A.Sc. and Ph.D. degrees in electrical engineering from Queen's University at Kingston, in 2008 and 2013, respectively.

From 2013 to 2015, he was an Assistant Professor with Queen's University at Kingston. In 2015, he joined Heriot-Watt University, Edinburgh, U.K., as an Assistant Professor, and became an Associate Professor in 2017. His research is supported by a H2020 Marie Sklodowska-Curie European Research Fellowship. He is currently a Senior Lecturer with the School of Engineering, University of Edinburgh, Edinburgh. He is a registered Professional Engineer with industrial experience as a computer programmer, and has designed 24 and 77 GHz automotive radar systems with Samsung and Magna Electronics. His industry experience also includes the design of high frequency surface-wave radar systems, professional software design and implementation for measurements in anechoic chambers for the Canadian Department of National Defence and the SLOWPOKE Nuclear Reactor Facility. He has also designed new compact multiple-input multiple-output antennas for wideband military communications, highly compact circularly polarized antennas for microsatellites with COM DEV International, and new wireless power transmission systems for Samsung. His research interests include surface waves, leaky-wave antennas, metasurfaces, UWB antennas, phased arrays, and CMOS integrated circuits.

Dr. Podilchak and his students have been the recipients of many best paper awards and scholarships; most notably research fellowships from the IEEE Antennas and Propagation Society, the IEEE Microwave Theory and Techniques Society, and the European Microwave Association. He also received a Postgraduate Fellowship from the Natural Sciences and Engineering Research Council of Canada and five Young Scientist Awards from the International Union of Radio Science. He received the Outstanding Dissertation Award for his Ph.D. from Queen's University at Kingston. In 2011, 2013, and 2020 received student paper awards at the IEEE International Symposium on Antennas and Propagation, and in 2012, the Best Paper Prize for Antenna Design at the European Conference on Antennas and Propagation for his work on CubeSat antennas, and in 2016, he received the European Microwave Prize for his research on surface waves and leaky-wave antennas. In 2017 and 2019, he was bestowed Visiting Professorship Awards at Sapienza University, Rome, Italy. He was recognized as an Outstanding Reviewer for the IEEE TRANSACTIONS ON ANTENNAS AND PROPAGATION from the IEEE Antennas and Propagation Society in 2014. He was also the Founder and the First Chairman of the IEEE Antennas and Propagation Society and the IEEE Microwave Theory and Techniques Society, Joint Chapter of the IEEE Kingston Section in Canada and Scotland. In recognition of these services, he was presented with an Outstanding Volunteer Award in May 2015 from IEEE. He currently serves as a Lecturer for the European School of Antennas and an Associate Editor for the *IET Electronic Letters*.

DIMITRIS E. ANAGNOSTOU (Senior Member, IEEE) received the B.S.E.E. degree from the Democritus University of Thrace, Greece, in 2000, and the M.S.E.E. and Ph.D. degrees from the University of New Mexico, Albuquerque, NM, USA, in 2002 and 2005, respectively.

From 2005 to 2006, he was a Postdoctoral Fellow with the Georgia Institute of Technology, Atlanta, GA, USA. In 2007, he joined the SD School of Mines and Technology, SD, USA, as an Assistant Professor and was later promoted to an Associate Professor with tenure. In 2016, he joined the Institute of Signals, Sensors and Systems, Heriot-Watt University, Edinburgh, U.K., as an Associate Professor. He has also worked with the Kirtland AFB, NM, USA, in 2011, as an AFRL Summer Faculty Fellow, and as Assistant Professor with the Democritus University of Thrace. He is currently supported by a European H2020 Marie Skłodowska-Curie Individual Fellowship on wireless sensing technologies. He has authored or coauthored more than 150 peer-reviewed journal and conference publications, one book chapter, and holds two U.S. patents on MEMS antennas and on optically scannable antennas. His research interests include antennas (reconfigurable, adaptive, miniaturized and electrically small, space/satellite, wearable), microwave circuits and packaging, radar sensing, 5G arrays, functional phase-change materials, such as VO2 for reconfigurable electronics and metasurfaces, direct-write electronics on organics, RF-MEMS, and applications of artificial neural networks, deep learning, and signal processing in electromagnetics and health care.

Dr. Anagnostou received the 2010 IEEE John D. Kraus Antenna Award, the 2011 DARPA Young Faculty Award from the U.S. Department of Defense, the 2014 Campus Star Award from the American Society for Engineering Education (ASEE), the 2017 Young Alumni Award from the University of New Mexico, the H2020 MSCA Fellowship, and four Honored Faculty Award from SDSMT. His students have also been recognized with IEEE and university awards (Engineering Prize at Heriot-Watt University, Best PhD Thesis at South Dakota School of Mines, and others). He serves or has served as an Associate Editor for the IEEE TRANSACTIONS ON ANTENNAS AND PROPAGATION (from 2010 to 2016), IEEE ACCESS, and *IET Microwaves, Antennas and Propagation*. He is a Guest Editor of the IEEE ANTENNAS AND WIRELESS PROPAGATION LETTERS (two Special Clusters), and *MDPI Electronics*. He is a member of the IEEE AP-S Educational Committee, and a Technical Program Committee member of the IEEE AP-S and EuCAP International Symposia. He is a member of the HKN Honor Society, ASEE, and the Technical Chamber of Greece as a registered Professional Engineer.

CONSTANTIN CONSTANTINIDES received the M.Sc. degree in signal and image processing in 2008, and the Ph.D. degree in image processing in 2012. He is an RF and Signal and Image Processing Engineer. After having studied in France, he went to Heriot-Watt University in Edinburgh, U.K., to work as a Researcher on leaky wave and compact antennas starting in 2015. He worked in space related projects, and then moved to Alba Orbital, Glasgow, to work as an Engineer in 2017, a company that designs pico-satellites. He currently works on designing and optimizing antennas for pico-satellites as well working on satellite night imaging techniques.

MUHAMMAD NAZRIN RAMLI was born in Perak, Malaysia, in 1991. He received the bachelor's and master's degrees in communication engineering from Universiti Malaysia Perlis, in 2015 and 2018, respectively. He is currently an Automation Engineer with Intel, Malaysia. His research interests include antennas and propagation, wearable antennas, flexible antennas, polymer antennas, and on-body communications. He was a First Place Recipient in the IEEE Malaysia Section Final Year Project Competition (Telecommunication Track) in 2015. He is also a Graduate Engineer registered with the Board of Engineers Malaysia.

HERWANSYAH LAGO was born in Sabah, Malaysia, in 1990. He received the B.Eng. and Ph.D. degrees in communication engineering from Universiti Malaysia Perlis, Malaysia, in 2013 and 2017, respectively. In 2017, he was appointed as a Postdoctoral Research Fellow with Universiti Teknikal Malaysia Melaka, Melaka, Malaysia. He is currently working as a Senior Lecturer with Universiti Malaysia Sabah. His research interests are in electronic telecommunications, especially in antenna structures, metamaterials, dielectric materials, RF, and microwave design.

PING JACK SOH (Senior Member, IEEE) was born in Sabah, Malaysia. He received the B.Eng. and M.Eng. degrees from Universiti Teknologi Malaysia, and the Ph.D. degree from KU Leuven, Belgium. He is currently an Associate Professor with the School of Computer and Communication Engineering, Universiti Malaysia Perlis (UniMAP), and a Research Affiliate with KU Leuven. From 2002 to 2004, he was a Test Engineer with Venture Corporation, and worked with Motorola Solutions, Malaysia, as a Research and Development Engineer in 2005. There, he worked on the characterization and testing of new two-way radio antennas and RF front-ends. From 2006, he joined SCCE-UniMAP as a Lecturer, and also served as the Deputy Director of the Centre for Industrial Collaboration from 2007 to 2009. He went on leave from UniMAP in 2009 to pursue his Ph.D and research attachment in KU Leuven, Belgium, where he was first as a Research Assistant from 2009 to 2013, then a Postdoctoral Research Fellow, from 2013 to 2014, and is currently a Research Affiliate with the ESAT-TELEMIC Research Division. Upon his return to UniMAP in 2014, he resumed his role as a Senior Lecturer, and concurrently served as the Deputy Dean of the university's Research Management and Innovation Center from 2014 to 2017. His involvement in several industrial research projects have resulted in a granted patent and five other filed patents. His research interests actively in areas of: wearable antennas, arrays, metasurfaces; on-body communication; electromagnetic safety and absorption; and wireless and radar techniques for healthcare applications. He was a recipient of the IEEE Antennas and Propagation Society Doctoral Research Award in 2012, the IEEE Microwave Theory and Techniques Society (MTT-S) Graduate Fellowship for Medical Applications in 2013, and the International Union of Radio Science (URSI) Young Scientist Award in 2015. He was also the Second Place Winner of the IEEE Presidents' Change the World Competition in 2013. Two of his (co)authored journals were awarded the IEEE AP/MTT/EMC Malaysia Joint Chapter's Best Paper Award in 2018 and 2019, and another two journals were also awarded the CST University Publication Award in 2012 and 2011. He is a Chartered Engineer registered with the U.K. Engineering Council; a Professional Technologist registered with the Malaysia Board of Technologist; and a member of IET and URSI. He also serves in the IEEE MTT-S Education Committee, and the MTT-S Meetings and Symposia Committee. He is currently an Associate Editor of the *International Journal of Numerical Modelling: Electronic Networks, Devices and Fields* (Wiley).